AGU PUBLICATIONS

Geochemistry, Geophysics, Geosystems

RESEARCH ARTICLE
10.1002/2015GC006153

Paleo-methane emissions recorded in foraminifera near the landward limit of the gas hydrate stability zone offshore western Svalbard

Giuliana Panieri[1], Carolyn A. Graves[2], and Rachael H. James[2]

[1]CAGE - Center of Arctic Gas Hydrate, Environment and Climate, Department of Geology, UiT University of Norway, Tromsø, Norway, [2]Ocean and Earth Science, National Oceanography Centre Southampton, University of Southampton, Southampton, UK

Key Points:
- Foraminifera serve as a template for carbonate precipitation in methane seep environments
- Foraminifera tests record fluctuations in methane seepage offshore western Svalbard
- There is a strong lithological control on methane seepage on the shelf off western Prins Karls Forland

Supporting Information:
- Supporting Information S1

Correspondence to:
G. Panieri,
giuliana.panieri@uit.no

Citation:
Panieri, G., C. A. Graves, and R. H. James (2016), Paleo-methane emissions recorded in foraminifera near the landward limit of the gas hydrate stability zone offshore western Svalbard, *Geochem. Geophys. Geosyst.*, *17*, 521–537, doi:10.1002/2015GC006153.

Received 23 OCT 2015
Accepted 19 JAN 2016
Accepted article online 23 JAN 2016
Published online 26 FEB 2016

Abstract We present stable isotope and geochemical data from four sediment cores from west of Prins Karls Forland (ca. 340 m water depth), offshore western Svalbard, recovered from close to sites of active methane seepage, as well as from shallower water depths where methane seepage is not presently observed. Our analyses provide insight into the record of methane seepage in an area where ongoing ocean warming may be fueling the destabilization of shallow methane hydrate. The $\delta^{13}C$ values of benthic and planktonic foraminifera at the methane seep sites show distinct intervals with negative values (as low as $-27.8‰$) that do not coincide with the present-day depth of the sulfate methane transition zone (SMTZ). These intervals are interpreted to record long-term fluctuations in methane release at the present-day landward limit of the gas hydrate stability zone (GHSZ). Shifts in the radiocarbon ages obtained from planktonic foraminifera toward older values are related to methane-derived authigenic carbonate overgrowths of the foraminiferal tests, and prevent us from establishing the chronology of seepage events. At shallower water depths, where seepage is not presently observed, no record of past methane seepage is recorded in foraminifera from sediments spanning the last 14 ka cal BP (^{14}C-AMS dating). $\delta^{13}C$ values of foraminiferal carbonate tests appear to be much more sensitive to methane seepage than other sediment parameters. By providing nucleation sites for authigenic carbonate precipitation, foraminifera thus record the position of even a transiently stable SMTZ, which is likely to be a characteristic of temporally variable methane fluxes.

1. Introduction

The contributions of different natural and anthropogenic sources of methane (CH_4), a potent greenhouse gas, to rising atmospheric methane concentrations remain poorly constrained [e.g., *Kirschke et al*., 2013; *Nisbet and Chappellaz*, 2009]. Seafloor methane seepage in the Arctic [e.g., *Sahling et al*., 2014; *Shakhova et al*., 2014; *Smith et al*., 2014; *Westbrook et al*., 2009] is of particular interest as climate warming is amplified in polar regions [e.g., *Parmentier and Christensen*, 2013] where many methane sources are climate sensitive [e.g., *Fisher et al*., 2011]. Understanding how Arctic seafloor methane seepage is likely to respond to further warming requires knowledge of the history and duration of the seepage observed today.

Methane hydrate, an ice-like compound which forms under high pressure and low temperature conditions from methane-saturated water, is a natural temperature-sensitive methane reservoir [*Hester and Brewer*, 2009]. Significant quantities of methane are stored as hydrate in marine sediments [e.g., *Dickens*, 2011; *Piñero et al*., 2013]. The volume of the gas hydrate stability zone (GHSZ) decreases in response to increasing ocean bottom water temperatures, causing a likely release of gaseous methane [e.g., *Dickens*, 2011; *Reagan and Moridis*, 2007]. Methane released from destabilizing hydrate and offshore permafrost in marine sediments may currently be bubbling into ocean bottom waters in the Arctic, North Atlantic, and North Pacific oceans [*Berndt et al*., 2014; *Hautala et al*., 2014; *Skarke et al*., 2014; *Shakhova et al*., 2014; *Westbrook et al*., 2009].

Seafloor methane seepage near the present-day landward limit of the GHSZ offshore western Svalbard, discovered in 2008 [*Westbrook et al*., 2009], has been suggested to be related to twentieth century temperature-driven hydrate dynamics [*Ferré et al*., 2012; *Reagan and Moridis*, 2009; *Sarkar et al*., 2012]. However, dating of authigenic carbonates at sites of present-day seepage indicates that the seeps have been active for at least 3000 years before present (BP) [*Berndt et al*., 2014]. Seasonal and decadal temperature

variability, superimposed on longer term trends, are expected to have produced cycles of methane accumulation as gas hydrate in shallow sediments during colder conditions followed by gas release as temperature increases [*Berndt et al*., 2014; *Marín-Moreno et al*., 2015].

A record of past marine environmental conditions is preserved in the calcite tests of foraminifera, which are unicellular marine organisms that build up protective exoskeletons through biomineralization. During the process of biologically controlled mineralization, foraminifera record chemical changes in their environment. For more than half a century [*Emiliani*, 1955], it has been accepted that the oxygen isotopic composition ($\delta^{18}O$) of foraminiferal carbonate tests reflects the oxygen composition of ambient water, thus providing a proxy for ocean temperature [*Epstein et al*., 1953; *Epstein and Mayeda*, 1953; *Urey et al*., 1951]. In addition, the carbon isotopic signature ($\delta^{13}C$) of calcite in benthic foraminifera reflects that of dissolved inorganic carbon (DIC) in the waters in which they calcified. The $\delta^{13}C$ of foraminifera is mainly controlled by global shifts related to changes in terrestrial vegetation and/or large-scale burial oxidation of sedimentary organic matter, and also by export production, respiration at depth, and age of deep water [e.g., *Rohling and Cooke*, 2002]. This explains its widespread use to reconstruct past changes in deep-water mass distribution and deep-water nutrient concentrations [*Kroopnick*, 1985]. Other influences on benthic foraminiferal $\delta^{13}C$ are due to the microhabitat effect, and the carbonate ion concentration effect [e.g., *Rohling and Cooke*, 2002].

In methane seep environments, the carbon isotopic signature of DIC in sediment pore waters and sometimes overlying seawater is dramatically ^{13}C-depleted ($\delta^{13}C_{DIC}$ can be lower than $-40‰$) [e.g., *Torres*, 2003] relative to the normal marine environment ($-1‰$ to $1‰$) [*Ravelo and Hillaire-Marcel*, 2007]. This is due to the metabolic coupling between archaea that oxidize methane that can have a microbial ($\delta^{13}C\text{-}CH_4 = -100‰$ to $-55‰$) and/or thermogenic origin ($\delta^{13}C\text{-}CH_4 = -55‰$ to $-40‰$) [*Whiticar*, 1999], and a variety of bacteria that reduce sulfate and produce sulfide and DIC. Under high pressure and low temperature conditions, this methane may have been in the hydrate phase. When methane rising from depth encounters pore water sulfate, anaerobic oxidation of methane (AOM; equation (1)) occurs in a distinct sediment interval termed the sulfate methane transition zone (SMTZ) [e.g., *Hoehler et al*., 1994]. Methane-derived DIC produced by AOM has a light isotopic signature [e.g., *Whiticar*, 1999], preserved in authigenic carbonates which precipitate due to local carbonate supersaturation at the SMTZ (equation (2)) [e.g., *Bayon et al*., 2007; *Berndt et al*., 2014; *Greinert et al*., 2001; *Ritger et al*., 1987]. The depth of the SMTZ is controlled by the methane flux [e.g., *Borowski et al*., 1996]. High methane fluxes result in AOM occurring close to the sediment-seawater interface, the establishment of benthic chemosynthetic communities including sulfide oxidizing bacterial mats, benthic aerobic oxidation of methane in ocean bottom waters (equation (3)), and the precipitation of authigenic carbonate crusts on the seafloor (equation (2))

$$CH_4 + SO_4^{2-} \rightarrow HS^- + HCO_3^- + H_2O \quad (1)$$

$$2HCO_3^- + Ca^{2+} \rightarrow CaCO_3 + CO_2 + H_2O \quad (2)$$

$$CH_4 + 2O_2 \rightarrow CO_2 + 2H_2O \quad (3)$$

The suitability of benthic and planktonic foraminifera for tracing past and present methane seepage activity is a subject of current debate. Deconvolution of the geochemical signals from primary foraminiferal calcite (formed during calcification) and secondary calcite overgrowths (precipitated on dead foraminifera in carbonate-saturated pore waters produced by AOM) is an active area of research [e.g., *Millo et al*., 2005a, 2005b; *Panieri et al*., 2012, 2014; *Pena et al*., 2005; *Martin et al*., 2010; *Torres et al*., 2010], but the possibility of using foraminifera carbon isotopic signatures to establish the location and timing of methane venting during the last deglaciation in the Arctic has also been explored [e.g., *Consolaro et al*., 2015; *Panieri et al*., 2014]. Preliminary data reveal a series of large negative excursions in benthic foraminiferal $\delta^{13}C$ interpreted to result from incorporation of ^{13}C-depleted carbon from methane emissions during the primary biomineralization of the tests, and likely ingestion of ^{13}C-depleted methanotrophic microbes [*Panieri*, 2006; *Rathburn et al*., 2003]. Additionally, in both benthic and planktonic foraminifera extremely negative $\delta^{13}C$ values (i.e., from -5% to -15%) have been interpreted to reflect precipitation of methane-derived authigenic carbonates as secondary overgrowths on the primary foraminifera tests [e.g., *Consolaro et al*., 2015; *Panieri et al*., 2014; *Torres et al*., 2010].

We present benthic and planktonic foraminiferal isotope data from sediment cores collected at the present-day GHSZ limit close to sites of active methane seepage offshore western Svalbard, as well as from cores

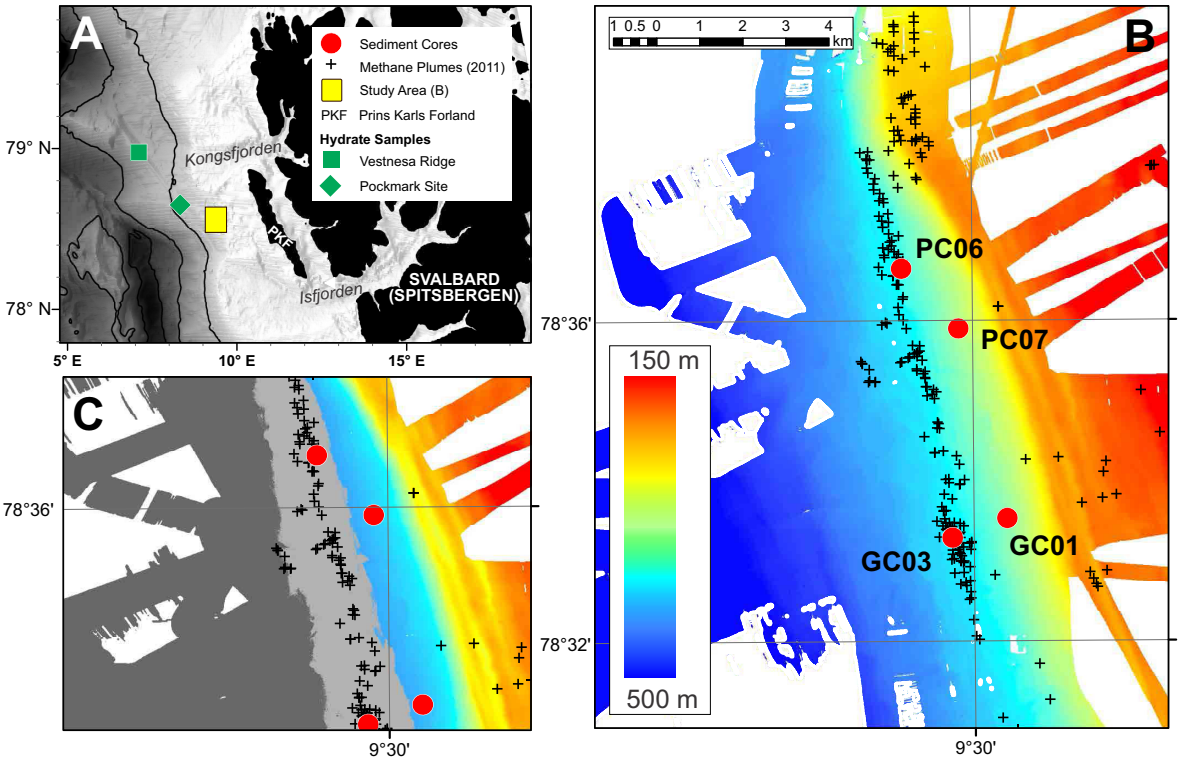

Figure 1. Map of study area offshore western Svalbard, showing (A) the study area, (B) locations of seafloor methane seeps mapped during cruise JR253, and (C) the seasonal limits (light grey area) of the present-day gas hydrate stability zone. Bathymetry in A is the GEBCO_08 Grid version 20100927 (http://gebco.net), contour interval is 1000 m (black lines), and in B and C are shipboard data from JR253. In C, light grey region indicates the maximum extent of the wintertime gas hydrate stability zone, and dark grey region sediments in which hydrate is expected to be stable year-round [*Berndt et al.*, 2014].

collected at shallower water depths that would have been located within the GHSZ in the past. We evaluate the potential of foraminiferal calcite as a tool for investigation of the history of seafloor methane seepage in this critically temperature-sensitive Arctic environment. We hypothesize that if seafloor methane seepage currently observed at the landward limit of the GHSZ results from recent retreat of the GHSZ from shallower waters, then a record of methane seepage would be preserved in these sediments. Our results demonstrate that foraminifera tests record long-term fluctuations in methane release at the present-day GHSZ limit, serving as nuclei for the formation of methane-derived authigenic carbonate. Both benthic and planktonic foraminifera exhibit negative values of $\delta^{13}C$ and we interpreted these anomalies as being due to secondary carbonate precipitation after the benthic and planktonic foraminifera were buried. While for benthic foraminifera there are still open questions related to their possibility to record methane during primary biomineralization [*Herguera et al.*, 2014; *Wollenburg et al.*, 2014], the planktonic foraminifera are not expected to record any signal from methane in the water column in this setting since the dissolved methane is rapidly dispersed and oxidized [*Graves et al.*, 2015; *Steinle et al.*, 2015]. However, our results do not elucidate any relationship between gas hydrate dissociation and seafloor gas emissions. No record of past methane seepage is recorded in foraminifera tests at shallower water depths. Finally, we show that radiocarbon ages are systematically shifted toward older values, due to precipitation of methane-derived authigenic carbonate overgrowth.

2. Geological and Oceanographic Setting

The western Svalbard continental margin consists of several cross-shelf troughs which were the drainage pathways of fast-flowing streams of ice sheets that reached the shelf several times in the Pliocene-Pleistocene, with the present-day shelf break marking their maximum expansion [*Solheim et al.*, 1996; *Svendsen et al.*, 1999; *Ingólfsson and Landvik*, 2013]. On the northwest Svalbard margin, the base of the prograding glacial wedge (seismic unit YP3) [*Eiken and Hinz*, 1993] was dated to approximately 2.7 Ma at ODP site 911 on the Yermak Plateau [*Mattingsdal et al.*, 2014].

Table 1. Locations of Sediment Cores[a]

Station ID	Date Sampled	Lat (°N)	Long. (°E)	Water Depth (m)	Core Length (cm)	SMTZ (m)
JR253-27-GC01	06/08/2011	78:33.54	9:32.09	340	209	4.0
JR253-53-PC06	11/08/2011	78:36.66	9:25.53	374	224	1.9
JR253-61-PC07	13/08/2011	78:35.91	9:29.10	323	137	5.5
JR235-78-GC03	15/08/2011	78:33.30	9:28.64	386	162	1.0

[a]GC, gravity core; PC, piston core. Depth of the SMTZ for cores GC01 and PC07 is derived by linear extrapolation of pore water sulfate profiles to zero sulfate.

The present-day landward limit of the GHSZ off western Svalbard is at ~400 m water depth (Figure 1c) [*Berndt et al*., 2014]. Seafloor methane seepage occurs west of Prins Karls Forland in the inter-fan region between the Isfjorden and Kongsfjorden cross-shelf troughs (Figure 1) [*Sahling et al*., 2014; *Westbrook et al*., 2009]. Seismic surveys indicate the presence of shallow gas in the upper continental margin sediments, and shallow methane hydrate deposits further offshore [*Chabert et al*., 2011; *Rajan et al*., 2012; *Sarkar et al*., 2012]. Gas migration appears to occur through permeable hemipelagic sediment sequences, which are variably capped by less permeable glacigenic sediments on the upper slope and shelf [*Rajan et al*., 2012; *Sarkar et al*., 2012; *Thatcher et al*., 2013]. The majority of methane seeps occur between 360 and 415 m water depth [*Sahling et al*., 2014], which corresponds to the depth range over which the landward limit of the GHSZ has shifted due to changes in bottom water temperatures in this region over the past ~30 years [*Ferré et al*., 2012; *Westbrook et al*., 2009]. Methane seepage in this area has been suggested to occur through permeable glacimarine strata and fractures [*Sarkar et al*., 2012].

The methane seeps that lie close to the present-day landward limit of the GHSZ (~385–395 m water depth) are associated with authigenic carbonates that have extremely negative carbon isotopic signatures, indicating incorporation of methane-derived carbon. U/Th dating of carbonates buried up to 240 cm depth in the sediments indicates that they precipitated between ~3 and 23 ka BP [*Berndt et al*., 2014]. Farther offshore, at water depths of ca. 1200 m, shallow methane hydrate and seafloor methane seepage are associated with faults providing a gas conduit through the GHSZ [*Hustoft et al*., 2009; *Plaza-Faverola et al*., 2015], and the foraminiferal calcite carbon isotopic record suggests intervals of seepage and quiescence for at least the last 23 ka which may be linked to climate events [*Consolaro et al*., 2015; *Panieri et al*., 2014].

Warm and saline Atlantic Water of the West Spitsbergen Current (WSC) [*Aagaard et al*., 1987] flows northward over the upper slope offshore Western Svalbard, while colder Arctic water of the East Spitsbergen Coastal Current flows northward over the shelf [*Saloranta and Svendsen*, 2001]. Historical temperature measurements in the WSC record multiple warming and cooling events since 1950, with overall warming since 1975 [*Ferré et al*., 2012; *Westbrook et al*., 2009]. *Spielhagen et al*. [2011] showed that the current Fram Strait ocean temperatures represent a maximum for the last 2000 years. A Holocene thermal maximum occurred at ~9.7–8.8 ka BP [*Ebbesen et al*., 2007]. The final deglaciation of the shelf occurred after the Younger Dryas stadial (11.7–12.9 ka BP) [*Rasmussen et al*., 2006], and was preceded by a glacial readvance at 14.5 ka BP at the transition into the Bølling-Allerød interstadial (15–14.6 ka BP) [*Jessen et al*., 2010, and references therein]. During the last glacial maximum (32–20.5 ka BP) full glaciation of the shelf occurred at ~24 ka BP [*Jessen et al*., 2010; *Müller and Stein*, 2014].

Along with temperature variability, glacial cycles were accompanied by local and global sea level changes due to ice volume changes and ice loading [*Ingólfsson and Landvik*, 2013; *Forman et al*., 2004]. Global sea level was at a minimum at 26 ka BP [*Jessen et al*., 2010]. Modern sea level was established at ~5.2 ka BP [*Werner et al*., 2013].

3. Materials and Methods

Sediment cores (PC, piston core and GC, gravity core) were collected during *RRS James Clark Ross* cruise 253 in August 2011. Locations are shown in Figure 1, and sampling sites are listed in Table 1. Two cores were collected within the area of seafloor methane seepage near the present-day landward limit of the GHSZ at 386 m water depth (GC03) and at 374 m water depth (PC06), and two cores (GC01 and PC07) were collected to the east in shallower waters (respectively, 340 and 323 m) where methane seepage is not presently observed. Hereafter, the cores are referred to as "GHSZ-limit" cores and "eastward" cores. The GHSZ-limit

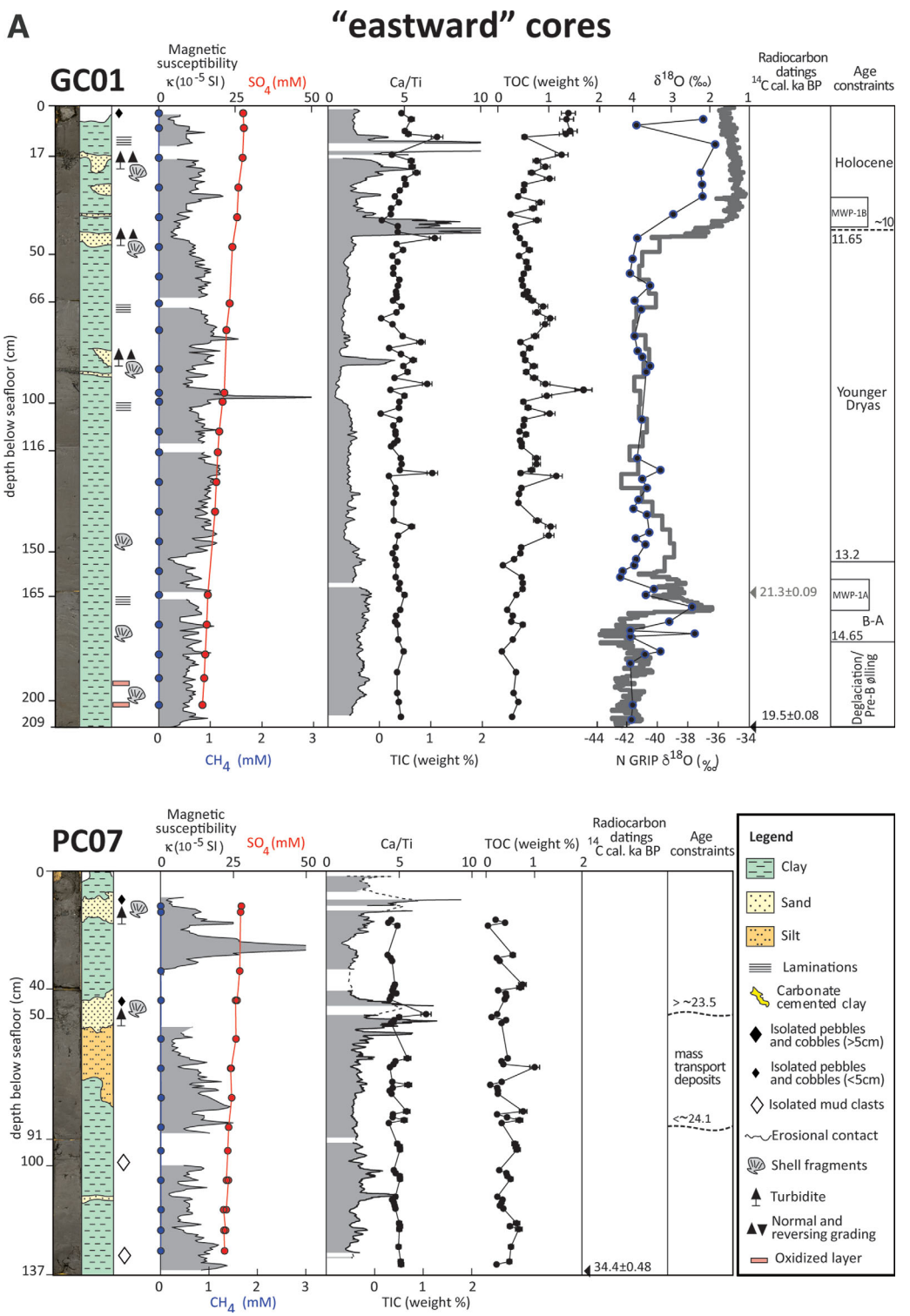

Figure 2. (A and B) Images and lithology of the investigated cores. Down-core logs of magnetic susceptibility, pore water methane (CH_4) and sulfate (SO_4) concentration, Ca/Ti ratio, TIC and TOC, and $\delta^{18}O$ of *N. pachyderma*. For GC01, $\delta^{18}O$ is tied to the NGRIP $\delta^{18}O$ curve. Radiocarbon dates (^{14}C cal ka BP) are indicated by black triangles when the $\delta^{13}C$ is within the range of normal marine values, in grey when dates have been discarded. The final column provides the stratigraphy derived for each core. Dashed horizontal line in (B) indicates the depth of the present-day sulfate-methane transition zone (SMTZ); see text for more details. The depth axis (numbers not multiples of 50) indicates the divisions between core sections.

cores were recovered within a few meters of active methane seeps identified by shipboard sonar and penetrated the depth of the present-day SMTZ (Figure 2), while the eastward cores were ~1 km from the nearest seeps and did not penetrate the SMTZ.

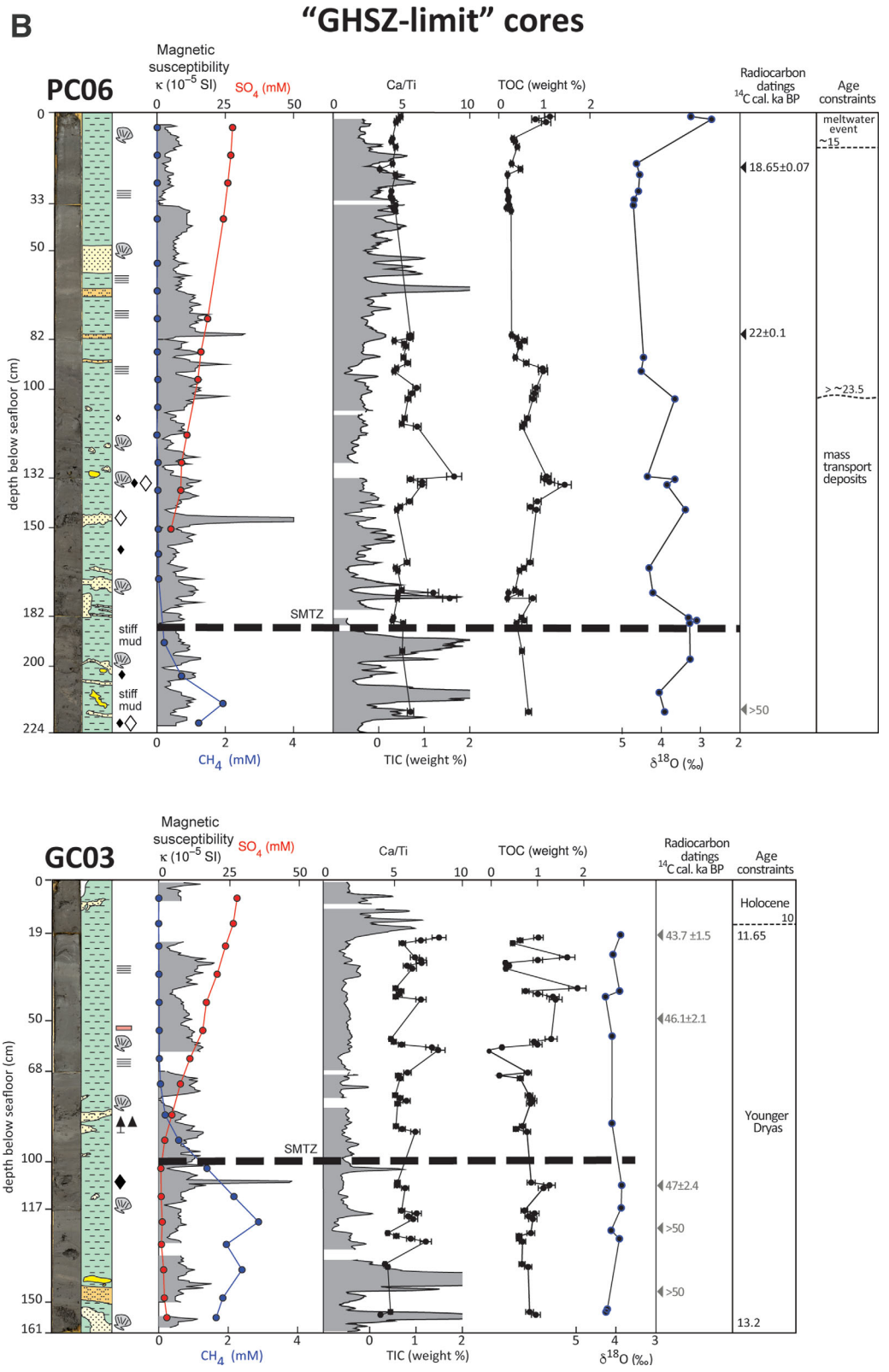

Figure 2. (continued)

3.1. Sample Processing and Analysis

Upon recovery, sediment cores were cut into ~50 cm sections and split lengthwise on deck. The working halves were immediately subsampled under a nitrogen atmosphere for methane, porosity, and pore fluid analysis. For methane analysis, ~3 mL of sediment was withdrawn using a cut-off plastic syringe and placed in a 20 mL crimp-seal glass vial containing 5 mL of 1 M sodium hydroxide; headspace was analyzed by gas chromatography onboard ship (Agilent 7890; analytical reproducibility of standards better than ±2%). Sediment methane concentrations were determined from headspace methane concentrations and porosity, calculated from the difference between the mass of wet sediment, and the mass of sediment after drying in an oven at ~60°C overnight. Pore waters were extracted by centrifugation under a nitrogen atmosphere, filtered through 0.2 μm cellulose acetate filters, and diluted by a factor of 200 with Milli-Q water. Sulfate concentrations were measured by ion chromatography (Dionex ICS250; reproducibility of replicate analyses better than ±1%).

Core sections were stored at 4°C onboard ship, and then at the British Ocean Sediment Core Research Facility (BOSCORF, National Oceanography Centre, Southampton, UK) where the archive half of each sediment core was logged for magnetic susceptibility (χ) on an XYZ Multi-Sensor Core Logger (Geotek) at 0.5 cm intervals and elemental abundance was determined using the ITRAX core-scanning X-ray fluorescence system (Cox Analytical) [*Croudace et al*., 2006] at 1 mm intervals (molybdenum X-ray tube, 30 s measurement time, 30 kV, 50 mA). Both data sets were processed to remove intervals where sudden changes in core surface height interfered with the detectors. Element abundances are presented as total counts normalized to titanium (Ti) as a proxy for terrigenous input [*Calvert and Pedersen*, 2007]. Total inorganic carbon (TIC) and total carbon (TC) contents of the sediments were determined by carbon coulometry (model CM5130, furnace module CM5120, acidification module CM5130) on ~50 mg of dried and ground sediment. Analytical reproducibility was better than ±10%. The concentration of total organic carbon (TOC) was determined by subtracting TIC from TC.

Prior to sampling, a visual core description was made on both the working and the archive halves. The descriptions focused on the occurrence of carbonates (nodules, pebbles, etc.) and silt and/or sand layers and lenses in the sediment sequence. All visible turbidite structures, such as grading, sharp lithology changes due to basal erosion, detritus compositions, and fossil remains, were noted. High quality photos were taken of the archive half of each core (Figure 2).

3.2. Processing for Micropaleontological Analyses

Sediment samples for micropalaeontological and stable isotope analysis were collected at 1 cm intervals. Samples were dried, then weighed, soaked in distilled water, and wet sieved at 44 μm. The residues were dried, and sieved at 300 and 500 μm.

The preservation of tests was assessed by scanning electron microscopy (SEM, Hitachi TM3030 table top microscope). From core PC06, benthic foraminifera tests from a sediment depth of 2 cm and planktonic foraminifera from 10 cm where δ^{13}C isotopic values are in the range of normal marine environments and benthic foraminifera tests from 111 and 173 cm below sea floor (bsf) and planktonic foraminifera from 173 cm where δ^{13}C instead indicate negative values outside of the range of normal marine environment were selected for SEM investigation. Special attention was paid to secondary overgrowths on the tests.

3.3. Stable Isotope and Radiocarbon Analyses

For oxygen and carbon stable isotope analyses, monospecific benthic and planktonic foraminifera samples were hand-picked from the 44 to 300 μm size fraction. For each interval, 3–10 (benthic) or 10–30 (planktonic) tests were analyzed after being gently crushed between clean glass plates to break open individual chambers and cleaned with methanol. The benthic species *Cassidulina neoteretis* Seidenkrantz, *Melonis barleanum* [*Williamson*, 1858], and *Nonionella labradorica* [*Dawson*, 1860], and the planktonic species *Neoglobquadrina pachyderma* [*Ehrenberg*, 1861] and *Globigerina bulloides* d'Orbigny were selected because they are abundant and common in this area [e.g., *Loeblich and Tappan*, 1953].

Stable isotope values (δ^{18}O and δ^{13}C) of both benthic and planktonic foraminifera were determined using a Europa GEO 20-20 mass spectrometer equipped with an automated carbonate preparation device at the University of Southampton, and a Thermo Finnigan MAT252 mass spectrometer coupled to a CarboKiel-II carbonate preparation device at the Serveis Cientifico-Técnics of the University of Barcelona. Results are

reported relative to the Vienna Pee Dee Belemnite (VPDB) and Vienna Standard Mean Ocean Water (VSMOW) standards in per mil (‰) notation for carbon and oxygen, respectively. External precision was better than $\pm 0.1‰$ for both $\delta^{13}C$ and $\delta^{18}O$ based on analysis of NBS-19.

Accelerator Mass Spectrometry (AMS) radiocarbon dating was performed on 11 samples of mixed planktonic foraminifera (predominantly *N. pachyderma* together with *G. bulloides*) from all the cores. A total weight of 1.3–2.8 mg of clean, well-preserved specimens was hand-picked from the 44–300 μm size fraction. The samples were selected avoiding the finer-grained layers formed of sand and gravel dispersed in a silty-mud matrix. The picked material was submitted for analysis at the National Ocean Sciences Accelerator Mass Spectrometry Facility (NOSAMS) radiocarbon laboratory at Woods Hole Oceanographic Institution (USA). Radiocarbon ages were calibrated using the marine calibration curve Marine13 (calibration curve maximum 46,806 year BP) [*Reimer et al*., 2013] which operates with a standard reservoir correction of −400 years [*Mangerud and Gulliksen*, 1975], and the program Calib 7.0 [*Stuiver et al.*, 2014]. A regional reservoir correction (ΔR) of 7 ± 11 years was applied, as recommended by Bondevik and Gullikesen in *Mangerud et al*. [2006], following *Panieri et al*. [2014] and *Consolaro et al*. [2015].

4. Results

4.1. Composition of Sediments

All cores contain multiple finer-grained layers formed of sand and gravel dispersed in a silty-mud matrix with sharp bottom and top contacts (Figure 2). The source of the gravel is exclusively terrigenous with abundant quartz, orthoclase, Ca-plagioclase, and lithic fragments. Silt layers and isolated mud clasts are present except in GC01. Carbonate nodules ~2–5 cm in size were recovered at the base of both GHSZ-limit cores (GC03 and PC06) and are absent from the other two cores.

Magnetic susceptibility (Figure 2) is very low overall (median: 13×10^{-5} SI). However, all cores contain strong peaks in magnetic susceptibility corresponding to sandy layers, though not all sandy layers are characterized by high magnetic susceptibility.

Ca/Ti ratios, which are indicative of carbonate content, are similar in all cores, with an average value of ~2. Intervals with higher Ca/Ti (>5) occur in the upper parts of GC01 and GC03, and in the lower part of PC06 and GC03 (Figure 2). Large broad peaks are typical of sandy intervals. GC03 contains a series of small Ca/Ti peaks which cannot be attributed to sandy layers, and correlate with depths from which carbonate concretions (2–5 cm diameter) were recovered. PC06 and PC07 both have slightly higher and much more variable calcium content, partially attributable to their larger proportion of discontinuous sand and silt layers.

The inorganic carbon content (TIC) of the eastward cores (GC01 and PC07) is relatively constant with depth at ~0.5 wt %, with isolated (single data point) peaks reaching 1.1% and dipping below 0.05%. The GHSZ-limit cores have higher and more variable TIC with an average of $0.6 \pm 0.3\%$, and a maximum value of 1.65%, corresponding to depth intervals containing visible authigenic carbonate nodules (Figure 2). The overall average sediment TOC content for all cores is 0.6 ± 0.3 wt % and is relatively constant with depth. TOC and TIC values are in broad agreement with previously reported data from nearby sites [e.g., *Elverhøi et al*., 1995; *Winkelmann and Knies*, 2005].

The GHSZ-limit cores penetrated the SMTZ identified by the depth where sulfate concentrations decrease below 1 mM, at 100 cm (bsf) in GC03 and 184 cm bsf in PC06. Above the SMTZ methane concentrations are less than 1 μM, while below they increase to >1.8 mM; note that some methane may have been lost due to degassing during recovery. The two eastward cores did not penetrate the SMTZ and if we assume that the sulfate concentrations continue to decrease linearly to the SMTZ this would occur at ca. 4 m bsf in GC01 and 5.5 m bsf in PC07.

4.2. Foraminiferal Stable Isotopes

Oxygen-isotope and carbon-isotope compositions of three benthic species (*C. neoteretis*, *M. barleeanum*, and *N. labradorica*) and one planktonic species (*N. pachyderma*) are listed in supporting information Tables S1–S4 and plotted in Figure 2 ($\delta^{18}O$ values of *N. pachyderma*) and Figure 3 ($\delta^{13}C$ values of all the species).

Eastward core GC01, the highest resolution record, shows low *N. pachyderma* $\delta^{18}O$ values of ~2‰ in near-surface sediments, and relatively steady values of ~4‰ throughout the deeper parts of the core with the

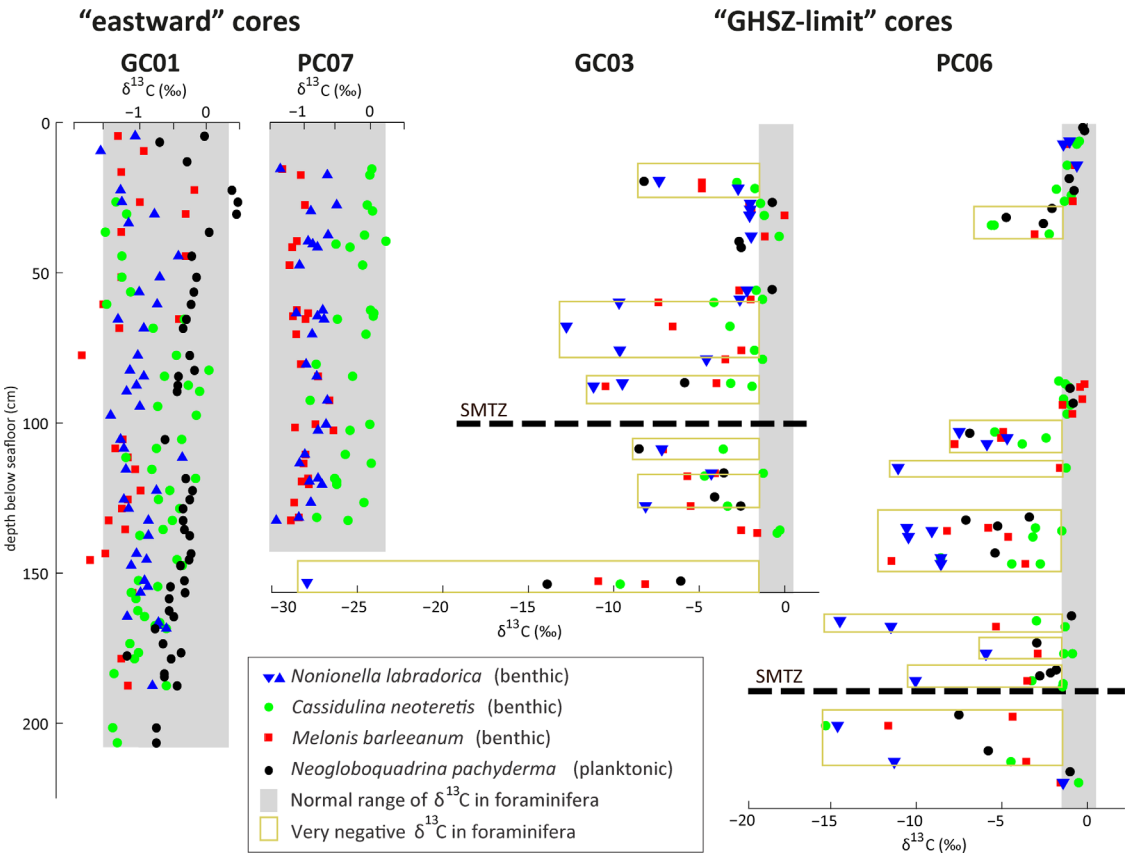

Figure 3. Benthic and planktonic foraminiferal $\delta^{13}C$ by species. For GHSZ-limit cores, dashed horizontal lines indicate the present-day depth of the SMTZ, vertical grey shaded region indicates the range of $\delta^{13}C$-values observed in the eastward cores, which are unaffected by methane seepage.

exception of an approximately 30 cm interval with lower values (~2.2‰) between 160 and 190 cm bsf (Figure 2a). *N. pachyderma* was not analyzed in the other eastward core (PC07). The GHSZ-limit core PC06 (Figure 2b), has $\delta^{18}O$ values of ~3‰ in near-surface sediments, below which values increase to 4.5‰ at ~25 cm bsf. Throughout the lower half of the core $\delta^{18}O$ oscillates between 4.5‰ and 3.5‰. In the other GHSZ-limit core (GC03), the $\delta^{18}O$ of *N. pachyderma* is relatively constant, with an average of ~4‰.

Stable carbon isotope data of *N. pachyderma* in GC01 (Figure 3) vary within a narrow range from −1‰ to 0.5‰, although one sample has lower $\delta^{13}C$ (−1.19‰), and a slightly higher $\delta^{18}O$ (2.39‰; Figure 2). In GHSZ-limit cores, sampled at lower depth resolution, planktonic carbon isotopic data are extremely ^{13}C-depleted (as low as −13.9‰) in some depth intervals, separated by intervals with normal marine $\delta^{13}C$ values (Figure 3). While some intervals show sharp variation in both $\delta^{18}O$ and $\delta^{13}C$, this is not always the case. There is no overall relationship between *N. pachyderma* $\delta^{13}C$ and $\delta^{18}O$.

Benthic foraminiferal $\delta^{18}O$ values show a similar pattern in all the cores and little variability (supporting information Tables S1–S4). The $\delta^{18}O$ values of *C. neoteretis* range from 3‰ to 5.5‰ in core GC01, from 4.2‰ to 5.6‰ in core PC07, from 3.1‰ to 5.2‰ in core PC06, and from 4.3‰ to 4.9‰ in GC03. The $\delta^{18}O$ values of *M. barleeanum* range from 2.4‰ to 4.5‰ in core GC01, from 3.7‰ to 5.2‰ in core PC07, from 3.3‰ to 5.1‰ in core PC06, and from 4.2 to 5 in core GC03. The $\delta^{18}O$ values of *N. labradorica* ranges from 3‰ to 4.5‰ in core GC01, in PC07 from 4.2‰ to 5.2‰, in PC06 from 4‰ to 5.3‰, and from 4‰ to 5.3‰ in GC03.

$\delta^{13}C$ values of benthic foraminifera (Figure 3) show a similar pattern to planktonic *N. pachyderma*: eastward cores exhibit a narrow range of values typical of the normal marine environment (−1.9‰ to 0.3‰), while benthic foraminifera from GHSZ-limit cores are significantly more ^{13}C-depleted (−27.8‰ to −0.02‰). In both GHSZ-limit cores, the magnitude of negative isotopic excursions increases with depth. Given the large variability with depth and the relatively low depth resolution, the available data set is not expected to record all transitions between normal and ^{13}C-depleted values. Samples near the depth of the present-day

Table 2. Radiocarbon Dates and $\delta^{13}C$ Values for Mixed Planktonic Foraminifera (*N. pachyderma* and *G. bulloides*) Samples Analyzed at the National Ocean Sciences Accelerator Mass Spectrometry Facility (NOSAMS) Radiocarbon Laboratory at Woods Hole Oceanographic Institution (USA)[a]

Core	Depth (cm)	NOSAMS Accession	Uncorrected AMS ^{14}C age (ka)	Calibrated age (cal yr BP, $\pm 2\sigma$ Median)	Mean Corrected Age (ka BP)	$\delta^{13}C$ (‰ VPDB)	Minimum % C-CH_4	Maximum % C-CH_4
GC01	164	OS-114142	18.05 ± 0.09	21,000–21,650	21.3 ± 0.09	−0.50	0	4
	213	OS-114143	16.6 ± 0.08	19,250–19,800	19.5 ± 0.08	−0.34	0	3
PC07	132	OS-114152	30.8 ± 0.48	33,600–35,300	34.4 ± 0.48	−0.60	0	4
PC06	20	OS-114149	15.8 ±0.07	18,500–18,800	18.65 ± 0.07	−1.16	0	6
	81	OS-114150	18.55 ± 0.10	21,700–22,300	22 ± 0.1	−1.69	1	8
	216	OS-114151	51.1 ± 5.6			−2.18	2	10
GC03	26	OS-114144	40.3 ± 1.5	41,400–46,200	43.7 ± 1.5	−1.68	1	8
	58	OS-114145	43.1 ± 2.1	43,000–49,800	46.1 ± 2.1	−3.24	5	14
	116	OS-114146	44.3 ± 2.4	43,600–50,000	47 ± 2.4	−4.92	9	20
	117	OS-114147	49.2 ± 4.4			−6.20	13	24
	153	OS-114148	>52 ± 7.4			−11.44	26	43

[a]Dates were determined using the Calib 7.0 software using the Marine13 calibration curve and reservoir correction of 7 ± 11 years. Minimum and maximum contributions of methane-derived carbon are calculated from a simple two-component mass balance, assuming methane-derived carbonate has $\delta^{13}C$ of between −41‰ and −27‰, and "normal marine" planktonic foraminiferal carbonate has $\delta^{13}C$ of between −1.2‰ and 0.5‰: $\delta^{13}C_{Observed} = [(\%C_{normal\ marine})(\delta^{13}C_{normal\ marine}) + (\%C_{methane\text{-}derived})\ (\delta^{13}C_{methane\text{-}derived})]/100$.

SMTZ have benthic foraminiferal $\delta^{13}C$ values ranging from normal (−1.45‰) to significantly ^{13}C-depeleted (−15‰). In the eastward cores, there is a consistent pattern between the three benthic species analyzed: values for *C. neoteretis* are more positive than for *N. labradorica*, which is in turn consistently more positive than *M. barleanum*. This pattern does not hold for GHSZ-limit cores. While *C. neoteretis* has generally more positive $\delta^{13}C$, in some intervals it has the more negative carbon isotopic signature. *N. labradorica* is generally isotopically more negative with intermediate $\delta^{13}C$ values observed for *M. barleanum*.

4.3. Radiocarbon Isotopes and $\delta^{13}C$ of Planktonic Foraminifera

Eleven radiocarbon dates were obtained for mixed planktonic foraminifera (predominantly *N. pachyderma* together with *G. bulloides*; Table 2 and Figure 2). For the eastward cores, in which planktonic and benthic $\delta^{13}C$ profiles reflect normal marine conditions, the dates are assumed to reflect stratigraphic ages. However, in GC01, the younger of the two radiocarbon dates is from the deeper sample. Neither sediment interval shows evidence of nonsequential sediment deposition, and $\delta^{13}C$ values reflect normal marine conditions. We reject the older date, because we cannot completely exclude that some specimens of *N. pachyderma* were reworked from older sediments that could have been involved in processes such as subglacial discharge from meltwaters.

The low $\delta^{13}C$ values (−1.68‰ to −11.44‰) and very old radiocarbon dates (uncorrected AMS ^{14}C ages 40.3 to >50 ka) in some GHSZ-limit core samples (PC06 and GC03; Table 2 and Figure 2) imply methane as the dominant carbon source for the carbonate overgrowth precipitated on the foraminiferal tests. The very low $\delta^{13}C$ values of foraminifera could be due to either organic matter oxidation or methane oxidized to CO_2 by methanotrophic archaea. Although the first possibility cannot be excluded, the second hypothesis seems to be more realistic in the case of the investigated site near the GHSZ-limit area where seafloor methane flares are abundant.

4.4. Chronology and Core Correlation

The obvious presence of on-going and past methane seepage and the shallow SMTZ in the GHSZ-limit cores has clearly affected the AMS ^{14}C ages, and prevents precise chronostratigraphic constraints from the available data. Very old radiocarbon dates (uncorrected AMS ^{14}C ages of 40.3 to >52 ka) with low $\delta^{13}C$ values (−1.68‰ to −11.44‰) reflect incorporation of fossil ^{14}C-free methane. Magnetic susceptibility records may also have been altered by the presence of sulphide at the STMZ [e.g., *Riedinger et al*., 2006], and the TIC content of the sediments and Ca/Ti ratio may reflect calcium carbonate precipitation related to AOM in addition to depositional variability. Furthermore, previous work on sediment cores in this area has revealed highly variable sedimentation rates and hiatuses, especially on the upper slope [e.g., *Elverhøi et al*., 1995; *Jessen et al*., 2010; *Winkelmann and Knies*, 2005; *Zamelczyk et al*., 2014].

For these reasons, we must derive local stratigraphic constraints for the upper continental margin off western Svalbard from the literature:

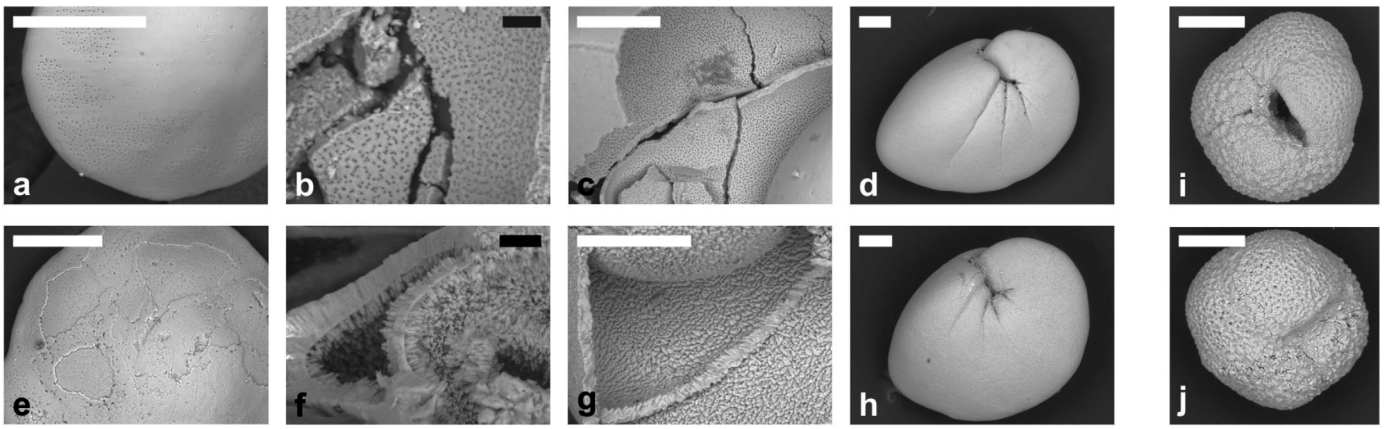

Figure 4. SEM images illustrating benthic and planktonic foraminifera shells from GHSZ-limit core PC06. (a, b) *C. neoteretis* and (c, d) *N. labradorica* from 2 cm bsf (normal δ^{13}C interval). In (a) and (d), the exterior shell is well preserved and the wall structure is pristine. (b) and (c) show the interior shell, with round pores and no alteration features (b), and a pristine wall (c). (e, f) *C. neoteretis* from 111 cm bsf and (g, h) *N. labradorica* from 173 cm bsf; both intervals are associated with extremely negative δ^{13}C values. All images show clear evidence of secondary carbonate overgrowths. Crystals of calcite are very well developed on the interior wall. (i, j) show *N. pachyderma* tests from (i; normal δ^{13}C interval) 10 cm and (j; extremely negative δ^{13}C) 173 cm bsf. White scale bars are all 100 μm, black are 10 μm.

i. A decrease in planktonic δ^{18}O from $\sim$4‰ to $\sim$2‰ at the beginning of the Holocene, $\sim$10 ka BP [*Andersen et al*., 1996; *Elverhøi et al*., 1995; *Jessen et al*., 2010; *Mangerud et al*., 1998].
ii. Spikes in δ^{18}O toward Holocene values at about 15 ka BP related to a local meltwater event, preceded by a decrease in TOC and simultaneous increase in $CaCO_3$ until about 20 ka BP [*Andersen et al*., 1996; *Elverhøi et al*., 1995; *Lucchi et al*., 2013].
iii. Mass transport deposits with low magnetic susceptibility at $\sim$24–23.5 ka BP consisting of dark coarse unsorted sediment with gravel sized clasts in a sticky, clayey, silty matrix [*Jessen et al*., 2010].

A general stratigraphy based on these constraints and the radiocarbon dates is shown in Figure 2. The NGRIP ice core δ^{18}O record [*Andersen et al*., 2004] is shown alongside GC01, as well as a general age model following *Panieri et al*. [2014]. The NGRIP record is tied to the GC01 data by: (1) the shift in *N. pachyderma* δ^{18}O values in the uppermost part of the core which is interpreted to represent the beginning of the Holocene, (2) the spikes in *N. pachyderma* δ^{18}O values which are interpreted to reflect Melt Water Pulse 1A (MWP-1A), a nearly instantaneous burst of terrigenous material at $\sim$14.6 ka associated with $\sim$20 m rise in sea level in $<$500 years [*Bard et al*., 1990; *Edwards et al*., 1993; *Fairbanks*, 1989; *Hanebuth et al*., 2000], during the Bølling-Allerød interstadial, and (3) the core-base radiocarbon date of 19.55 $\pm$ 0.08 cal ka BP. We assume a linear sedimentation rate and that the core top represents the present day. The resulting estimated sedimentation rates are 4 cm kyr^{-1} during the Holocene, and $\sim$90 cm kyr^{-1} during the Younger Dryas stadial. The sedimentation rate for the Holocene is in good agreement with those previously reported for the upper Svalbard continental margin [*Andersen et al*., 1996; *Elverhøi et al*., 1995].

Age constraints for the other three cores are poor. In PC07, a thick sand and silt interval is interpreted to represent mass transport deposits from $\sim$24 to 23.4 ka BP, in agreement with the core bottom radiocarbon date of 34 $\pm$ 0.48 cal ka BP. This gives a low average sedimentation rate of 4 cm kyr^{-1}, which may imply that upper Holocene and Younger Dryas sediments are missing. This is consistent with the stratigraphy of nearby cores, which also show significant sediment hiatuses at the surface [*Elverhøi et al*., 1995; *Jessen et al*., 2010; *Rebesco et al*., 2013].

In PC06, we also infer that surface sediments have been lost either during sampling or due to winnowing by high bottom water currents as described by *Winkelmann and Knies* [2005]. Taking the upper sediment radiocarbon date (18.65 $\pm$ 0.07 cal ka BP) with normal δ^{13}C ($-$1.16‰) to be unaffected by methane-derived carbon, we interpret the low δ^{18}O values of *N. pachyderma* in the upper part of the core to represent the end of MWP-1A during the Bølling-Allerød interstadial ($\sim$15 ka BP). This interval could represent the laminated sediments 14.7–14.38 cal ka BP indicated by *Jessen et al*. [2010]. According to these authors, the underlying thick sediment interval of stiff mud containing numerous shells and isolated pebbles should represent the mass transport deposits of $\sim$24 to 23.4 ka BP. The interval is characterized by several thin sand

and silt beds intercalated with hemipelagic mud that we interpret as thin-bedded turbidite deposits. The age at the base of the core, which is beyond the detection limit of ^{14}C, is clearly affected by methane-derived carbon since the $\delta^{13}C$ value of planktonic foraminifera is very low and the sample is close to the present-day SMTZ, and does not provide a reliable chronostratigraphic constraint.

Finally, in GC03, where all samples used for dating exhibit very negative $\delta^{13}C$, all radiocarbon dates show a significant contribution from old, ^{14}C-free methane. The low resolution *N. pachyderma* $\delta^{18}O$ record (due to very few specimens of foraminifera) appears to indicate that Holocene sediments are either absent or restricted to the upper ~20 cm. High calcium content (Ca/Ti) in the upper 20 cm is consistent with the Holocene and may be indicative of good recovery of surface sediments. Conversely, the very old radiocarbon age associated with near-normal $\delta^{13}C$ at 26 cm depth apparently indicates a significant loss of recent sediments; if the carbonate is only 1–8% methane-derived carbon then the actual sediment date should be very close to the measured value (43.7 ± 1.5 cal ka BP). This seems unlikely based on records from nearby cores which are consistent with U/Th ages in carbonates from a core recovered less than 100 m away (13–11 ka at 60–120 cm depth) [*Berndt et al.*, 2014], assuming the carbonates (which have $\delta^{13}C$ values of $<-35‰$), reflect authigenic carbonate precipitation driven by anaerobic methane oxidation close to the sediment surface.

5. Discussion

5.1. Mass Balance Approach for Interpreting Isotopic Anomalies in Foraminifera

For GHSZ-limit cores, assuming that planktonic foraminiferal calcite carbon consists of a mixture of "normal" surface ocean DIC and diagenetic overprinting with methane-derived carbon, the measured radiocarbon activity and $\delta^{13}C$ value must reflect the relative proportions of the two carbon sources. For the diagenetic carbonate end-member, we use data from bulk sediments and carbonate concretions (including solid filling in a gastropod) from the seep region ($\delta^{13}C$: $-27‰$ to $-41‰$) [*Berndt et al.*, 2014]. The primary foraminiferal calcite end-member is taken from the maximum and minimum $\delta^{13}C$ values for *N. pachyderma* in GC01: $-1.2‰$ and $0.5‰$. The resulting minimum and maximum contributions of methane-derived carbonate diagenetic overprinting on the planktonic foraminiferal samples used for radiocarbon dating are given in Table 2.

Simple mass balance consideration (explanation in the caption of Table 2) of the radiocarbon data yields two interesting results. The first is that samples with the same $\delta^{13}C$, and therefore the same assumed contribution from methane-derived carbon, have dramatically different ages: 43.7 ± 1.5 cal ka BP ($\delta^{13}C = -1.68‰$) at 26 cm depth in GC03, and 22 ± 0.1 cal ka BP ($\delta^{13}C = -1.69‰$) at 81 cm depth in PC06 (Table 2). The younger PC06 date shows the small methane-derived carbon effect expected from the $\delta^{13}C$ data. The very old GC03 date appears to suggest a significant contribution of methane-derived carbon, which is not consistent with its $\delta^{13}C$ value. We have to take into account that since the measured species (*N. pachyderma* and *G. bulloides*) are the same in all samples, the primary $\delta^{13}C$ should be the same ($\delta^{13}C$ from $-0.5‰$ to $1‰$) [*Jessen et al.*, 2010]. It seems unlikely that the sediments at this site reflect erosion or a depositional hiatus spanning the entire ages of the recovered sediments in the two eastward cores. The second noteworthy result of the mass balance analysis is that despite the expected overprinting of methane-derived fossil ^{14}C signature on the stratigraphic record, both GHSZ-limit cores show increasing age with depth. This is consistent with the accompanying decrease in $\delta^{13}C$ values, and may simply reflect that by chance, the eight samples selected for dating (5 in GC03 and 3 in PC06) were more negative at depth (Figure 2).

5.2. Evidence for Methane Transport Through the Sediments

The calcium content (Ca/Ti; Figure 2) of the GHSZ-limit cores is affected by calcium carbonate precipitation at the SMTZ (equation (2)) since the amount of calcium increases in this depth interval. This is particularly evident at the base of core PC06 (between ca. 175 and 210 cm bsf) where Ca/Ti peaks occur at the present-day SMTZ (at 184 cm bsf), and carbonate nodules were also present. In the same depth interval (between ca. 184 cm bsf to the base of the core), foraminifera exhibit a strong negative anomaly in $\delta^{13}C$. In contrast, in the eastward cores where the SMTZ is not present, Ca/Ti is relatively low and stable with peaks restricted to sandy intervals.

Hydrogen sulfide produced by AOM at the SMTZ promotes the dissolution of detrital magnetite. This reduction in sediment solid phase (oxyhydr)oxides can cause a drawdown in the magnetic susceptibility profiles

across the SMTZ [e.g., *Dewangan et al*., 2013; *Neretin et al*., 2004; *Riedinger et al*., 2005]. The change in magnetic susceptibility depends on both the availability of detrital magnetite, and the amount of time that the SMTZ is fixed in a given sediment interval, the latter determined by a combination of sedimentation rates and methane fluxes. We observe no drawdown of magnetic susceptibility across the present-day SMTZ depth in the GHSZ-limit cores, nor any difference in magnetic susceptibility between the GHSZ-limit cores and the eastward cores in which sediments appear not to have been exposed to AOM (Figure 2). Despite lack of evidence for alteration of magnetic susceptibility by AOM, there is no stratigraphic correlation of magnetic susceptibility between cores.

In this investigation, δ^{13}C values of foraminifera carbonate tests appear to be much more sensitive to methane seepage than other sediment parameters. By providing nucleation sites for authigenic carbonate precipitation, foraminifera thus record the presence of even a transiently stable SMTZ, which is likely to be characteristic of the temporally variable methane fluxes near the limit of hydrate stability in marine sediments. At the SMTZ, the metabolic coupling between methane oxidizing archaea and sulfate reducing bacteria produces sulfide and dissolved inorganic carbon, including the potential for large increases in carbonate alkalinity that drive pervasive carbonate precipitation. It is likely that only high and sustained methane fluxes, which fix the SMTZ in a given sediment interval, are able to modify intrinsic properties of marine sediments.

5.3. Record of Past Methane Fluxes Offshore Western Svalbard

The extremely light foraminiferal calcite δ^{13}C values in sediments close to the GHSZ limit (Figure 3) clearly indicate that both benthic and planktonic foraminifera record methane seepage on the upper continental margin off western Svalbard. The incorporation of light methane-derived carbon may partly occur during primary calcification of benthic foraminifera in sediments affected by methane seepage [e.g., *Rathburn et al*., 2003; *Hill et al*., 2004; *Panieri et al*., 2014], but also during secondary carbonate precipitation on the outer part of the foraminiferal test caused by AOM [*Torres*, 2003, *Torres et al*., 2010; *Consolaro et al*., 2015]. Secondary overgrowths via AOM can be deposited in near-surface sediments during times of high methane flux, but also at a subsurface SMTZ when methane fluxes are insufficient to bypass the microbial oxidation filter and reach the sediment-water interface. Normal *N. pachyderma* δ^{13}C values in eastward core GC01 in contrast with exceptionally low *N. pachyderma* δ^{13}C values in cores from the GHSZ limit which cannot be produced by biomineralization [cf. *Millo et al*., 2005a], so much of this signal must be a result of secondary authigenic carbonate precipitation. This is confirmed by SEM investigation of foraminiferal tests (Figure 4): we observed that specimens from the eastward cores and those from GHSZ-limit cores with normal marine δ^{13}C values have pristine test walls, whereas specimens from the GHSZ-limit cores with very low δ^{13}C values have internal and external overgrowths of secondary calcite crystals and patina.

The presence of intervals with very low benthic foraminiferal δ^{13}C both above and below the depth of the present-day SMTZ indicates that methane fluxes in GHSZ-limit cores have varied in the past. During periods of colder bottom water temperatures, the cores would be located within the GHSZ so methane seepage would be expected to be blocked by hydrate formation in the sediments wherever pore fluids are methane-saturated. During periods of warming, the sampled sediments would be outside the GHSZ. Methane hydrate accumulated in near-surface sediments as hydrate would therefore dissociate, fuelling a high methane flux and shallow SMTZ depths near or at the seafloor. If warm conditions persist, all of the hydrate will dissociate, the sediment methane flux will decrease, and the SMTZ would shift to deeper depths. As we are unable to provide firm stratigraphic controls for these cores due to the presence of carbonate overgrowths on foraminiferal tests, we cannot relate periods of high versus low methane flux to specific climate events. Nevertheless, the oscillations in the depth of the SMTZ that we observe in our records imply that temperature-driven changes in gas hydrate extent are likely to play a role.

The absence of light methane-derived carbonate in the eastward cores, which are expected to have been located within the GHSZ at some point since the last glacial maximum [*Ferré et al*., 2012; *Thatcher et al*., 2013], implies either that (1) methane seepage has not occurred at these sites over the last ~30 ka, or (2) past methane emissions in these sediments were weak or short-lived, such that authigenic carbonate did not accumulate at the SMTZ even as secondary overgrowth on foraminifera tests. As the continental slope in this area is underlain by numerous unstratified units of apparent glacial origin, which would be very poorly sorted and have a very low permeability [*Sarkar et al*., 2012; *Thatcher et al*., 2013], we suggest that it is most likely that seepage

has not occurred at either of the eastward core sites (now or in the past) because the cores were taken in or above geological formations that are aquitards, and thus preclude methane seepage. If this is correct, then it means that on some parts of the western Svalbard margin, lithological constraints on fluid flow pathways in low-permeability shallow sediments play a critical role in regulating sites of methane seepage. Therefore, temperature driven shifts in the size of the GHSZ are unlikely to be the most important control of sites of seafloor methane seepage despite the alignment of present-day seafloor seeps with a segment of the landward limit of the GHSZ. In support of this, methane seeps to the north of our study area are offset to slightly shallower water depths (<300 m) [*Sarkar et al*., 2012; *Rajan et al*., 2012], and further north still there is no evidence for methane release at the landward limit of the GHSZ [*Sahling et al*., 2014].

6. Conclusions

We have presented foraminiferal isotope, sediment geochemistry, and magnetic susceptibility from four sediment cores collected offshore western Svalbard. Two cores were collected from sediments where methane hydrate is hypothesized to have destabilized within at least the last ~30 years and methane is currently being released at the seafloor, and two cores were collected from shallower waters depths which would have been within the GHSZ in the past (at some point since the last glacial maximum).

Benthic and planktonic foraminifera $\delta^{13}C$ provide a clear record of methane seepage in sediments collected from close to the depth of the landward limit of the present-day GHSZ. Negative shifts in $\delta^{13}C$ values, separated by at least one sample with normal marine values, occur in distinct intervals at both the present-day SMTZ and in deeper and shallower sediment intervals, recording long-lived but highly variable methane fluxes. The negative $\delta^{13}C$ values could be affected by carbon from organic matter oxidation, since the site is relatively shallow and close to the continental margin, and by migration and oxidation of methane. In addition, the magnitude of the $\delta^{13}C$ anomaly may be indicative of different types of methane seepage: from very slow diffusion through the sediments leading to "inter-granular seepages" or "micro-seepages" [*Damm et al*., 2005] to vigorous methane gas fluxes as observed at the main ridge of the Forlandet moraine complex [*Sahling et al*., 2014]. Precise timing of the methane emissions is difficult to establish, but it seems likely that they occurred after the sediments were deposited as they are affected by precipitation of carbonate overgrowth on foraminifera tests.

In this setting, high methane fluxes in the sediments appear to affect the magnetic susceptibility, the Ca/Ti ratio, and the total inorganic carbon concentration of the sediments. However, the variability in methane fluxes and thus the position of the SMTZ within the sediments means that these parameters are poor proxies for methane seepage. Moreover, the passage of methane through the sediments, and AOM, make it extremely difficult to establish the stratigraphy (e.g., via magnetic susceptibility) or chronostratigraphy (^{14}C dating) of the sediments. Methane-derived authigenic carbonate contains carbon from fossil methane, and its precipitation on planktonic foraminiferal tests leads to extremely old radiocarbon dates which are inconsistent with available stratigraphic constraints. The presence of methane-derived carbonate is confirmed by extremely low $\delta^{13}C$ values, but the radiocarbon ages of samples with identical $\delta^{13}C$ differ significantly. The effect of methane-derived carbon on ^{14}C warrants further investigation.

The absence of any evidence for methane seepage within the sediments recovered at shallower depths, where gas hydrate would have been stable during past intervals of lower bottom water temperatures [*Ferré et al*., 2012], implies that dissociation of gas hydrate is not the primary control on seafloor methane seepage on the upper continental margin. Rather, we suggest that there is a strong lithological control on methane seepage. A more extensive coring survey is required to determine if seafloor seepage has always been absent at these water depths, together with seismic surveys to determine the links between the sedimentary facies and the subsurface gas distribution and gas migration pathways. As Arctic Ocean bottom waters continue to warm, such surveys are imperative to establish the potential for methane release to the water column due to hydrate dissociation.

Acknowledgments
This work was funded by the UK Department of Energy and Climate Change (DECC) as part of the Natural Environment Research Council (NERC) Arctic Research Programme, and partly supported by the Research Council of Norway through its Centres of Excellence funding scheme, project 223259, and by PNRA Project FORMAT. G.P. thanks A. Asioli for picking of planktonic foraminifera in core GC01. Jürgen Mienert, Graham Westbrook, Andreia Plaza Faverola, Jan Sverre Laberg, Joel Johnson, and the two reviewers Ruth Martin and Thomas Pape provided valuable comments on earlier versions of this paper. C.G. was supported by a PhD Studentship from the University of Southampton, and Postgraduate Scholarships from the Natural Sciences and Engineering Research Council of Canada (NSERC PGSM, PGSD3). Collaboration was supported by the European Concerted Research Action COST Action ES0902 PERGAMON. The data are stored at the Centre for Arctic Gas Hydrate, Environment and Climate data repository and are accessible by contacting fabio.sarti@uit.no.

References

Aagaard, K., A. Foldvik, and S. R. Hillman (1987), The West Spitsbergen Current: Disposition and water mass transformation, *J. Geophys. Res.*, *92*, 3778–3784.

Andersen, E. S., T. M. Dokken, A. Elverhøi, A. Solheim, and I. Fossen (1996), Late Quaternary sedimentation and glacial history of the western Svalbard continental margin, *Mar. Geol.*, *133*, 123–156.

Andersen, K. K., et al. (2004), High-resolution record of Northern-Hemisphere climate extending into the last interglacial period, *Nature*, *431*, 147–151.
Bard, E., H. Bruno, R. G. Fairbanks, and A. Zindler (1990), Calibration of the ^{14}C timescale over the past 30,000 years using mass spectrometric U-Th ages from Barbados corals, *Nature*, *345*, 405–410.
Bayon, G., C. Pierre, J. Etoubleau, M. Voisset, E. Cauquil, T. Marsset, N. Sultan, E. Le Drezen, and Y. Fouquet (2007), Sr/Ca and Mg/Ca ratios in Niger Delta sediments: Implications for authigenic carbonate genesis in cold seep environments, *Mar. Geol.*, *241*, 93–109.
Berndt, C., et al. (2014), Temporal constraints on hydrate-controlled methane seepage off Svalbard, *Science*, *343*, 284–287.
Borowski, W. S., C. K. Paull, and W. Ussler (1996), Marine pore-water sulfate profiles indicate in situ methane flux from underlying gas hydrate, *Geology*, *24*, 655–658.
Calvert, S., and T. Pedersen (2007), Elemental proxies for palaeoclimatic and palaeoceanographic variability in marine sediments: Interpretation and applications, in *Proxies in Late Cenozoic Paleoceanography*, edited by C. Hillaire-Marcel and d. V. Anne, pp. 567–644, Elsevier, Amsterdam.
Chabert, A., T. A. Minshull, G. K. Westbrook, C. Berndt, K. E. Thatcher, and S. Sarkar (2011), Characterization of a stratigraphically constrained gas hydrate system along the western continental margin of Svalbard from ocean bottom seismometer data, *J. Geophys. Res.*, *116*, B12102, doi:10.1029/2011JB008211.
Consolaro, C., T. L. Rasmussen, G. Panieri, J. Mienert, S. Bünz, and K. Sztybor (2015), Carbon isotope ($\delta^{13}C$) excursions suggest times of major methane release during the last 14 kyr in Fram Strait, the deep-water gateway to the Arctic, *Clim. Past*, *11*, 669–685.
Croudace, I. W., A. Rindby, and R. G. Rothwell (2006), ITRAX: description and evaluation of a new X-ray core scanner, in edited by R. G. Rothwell, New ways of looking at sediment cores and core data, Geol. Soc. Sp. Publ., *267*, 51–63.
Damm, E., A. Mackensen, G. Budéus, E. Faber, and C. Hanfland, (2005), Pathways of methane in seawater: Plume spreading in an Arctic shelf environment (SW-Spitsbergen), *Cont. Shelf Res.*, *25*, 1453–1472.
Dewangan, P., N. Basavaiah, F. K., Badesab, A. Usapkar, A. Mazumdar, R. Joshi, and T. Ramprasad (2013), Diagenesis of magnetic minerals in a gas hydrate/cold seep environment off the Krishna-Godavari basin, Bay of Bengal, *Mar. Geol.*, *340*, 57–70.
Dickens, G. R. (2011), Down the rabbit hole: Toward appropriate discussion of methane release from gas hydrate systems during the Paleocene-Eocene thermal maximum and other past hyperthermal events, *Clim. Past*, *7*, 831–846.
Ebbesen, H., M. Hald, and T. H. Eplet (2007), Lateglacial and early Holocene climatic oscillations on the western Svalbard margin, European Arctic, *Quat. Sci. Rev.*, *26*, 1999–2011.
Edwards, R. L., J. W. Beck, G. Burr, D. Donahue, J. Chappell, A. Bloom, E. Druffel, and F. Taylor (1993), A large drop in atmospheric $^{14}C/^{12}C$ and reduced melting in the Younger Dryas, documented with ^{230}Th ages of corals, *Science*, *260*, 962–962.
Eiken, O., and K. Hinz (1993), Contourites in the Fram Strait, *Sediment. Geol.*, *82*, 15–32.
Elverhøi, A., E. S. Andersen, T. Dokken, D. Hebbeln, R. Spielhagen, J. I. Svendsen, M. Sørflaten, A. Rørnes, M. Hald, and C. F. Forsberg (1995), The growth and decay of the Late Weichselian ice sheet in western Svalbard and adjacent areas based on provenance studies of marine sediments, *Quat. Res.*, *44*, 303–316.
Emiliani, C. (1955), Pleistocene temperatures, *J. Geol.*, *63*, 538–578.
Epstein, S., and T. Mayeda (1953), Variation of O^{18} content of waters from natural sources, *Geochim. Cosmochim. Acta*, *4*, 213–224.
Epstein, S., R. Buchsbaum, H. A. Lowenstam, and H. C. Urey (1953), Revised carbonate-water isotopic temperature scale, *Geol. Soc. Am. Bull.*, *64*, 1315–1326.
Fairbanks, R. G. (1989), A 17,000-year glacio-eustatic seal level record: Influence of glacial melting rates on the Younger Dryas event and deep-ocean circulation, *Nature*, *342*, 637–642.
Ferré, B., J. Mienert, and T. Feseker (2012), Ocean temperature variability for the past 60 years on the Norwegian-Svalbard margin influences gas hydrate stability on human time scales, *J. Geophys. Res.*, *117*, C10017, doi:10.1029/2012JC008300.
Fisher, R. E., et al. (2011), Arctic methane sources: Isotopic evidence for atmospheric inputs, *Geophys. Res. Lett.*, *38*, L21803, doi:10.1029/2011GL049319.
Forman, S. L., D. J. Lubinski, O. Ingolfsson, J. J. Zeeberg, J. A. Snyder, M. J. Siegert, and G. G. Matishov (2004), A review of postglacial emergence on Svalbard, Franz Josef Land and Novaya Zemlya, northern Eurasia, *Quat. Sci. Rev.*, *23*, 1391–1434.
Graves, C. A., L. Steinle, G. Rehder, H. Niemann, D. P. Connelly, D. Lowry, R. E. Fisher, A. W. Stott, H. Sahling, and R. H. James (2015), Fluxes and fate of dissolved methane released at the seafloor at the landward limit of the gas hydrate stability zone offshore western Svalbard, *J. Geophys. Res. Oceans*, *120*, 6185–6201, doi:10.1002/2015JC011084.
Greinert, J., G. Hobrmann, and E. Seuess (2001), Gas hydrate associated carbonates and methane-venting at hydrate rdige: Classification, distribution, and origin of authigenic lithologies, in *Natural Gas Hydrates: Occurrence, Distribution, and Detection*, edited by C. K. Paull and W. P. Dillon, pp. 99–113, AGU, Washington, D. C.
Hanebuth, T., K. Stattegger, and P. M. Grootes (2000), Rapid flooding of the Sunda Shelf: a Late-Glacial sea-level record, Science, *288*, 1033–1035.
Hautala, S. L., E. A. Solomon, H. P. Johnson, R. N. Harris, and U. K. Miller (2014), Dissociation of Cascadia margin gas hydrates in response to contemporary ocean warming, *Geophys. Res. Lett.*, *41*, 8486–8494, doi:10.1002/2014GL061606.
Hester, K. C., and P. G. Brewer (2009), Clathrate hydrates in nature, *Annu. Rev. Mar. Sci.*, *1*, 303–327.
Herguera, J. C., C. K. Paull, E. Perez, W. Ussler III, and E. Peltzer (2014), Limits to the sensitivity of living benthic foraminifera to pore water carbon isotope anomalies in methane vent environments, *Paleoceanography*, *29*, 273–289, doi:10.1002/2013PA002457.
Hill, T. M., J. P. Kennett, and D. L. Valentin (2004), Isotopic evidence for the incorporation of methane-derived carbon into foraminifera from modern methane seeps, Hydrate Ridge, Northeast Pacific, *Geochim. Cosmochi Acta*, *68/22*, 4619–4627.
Hoehler, T. M., M. J. Alperin, D. B. Albert, and C. S. Martens (1994), Field and laboratory studies of methae oxidation in an anoxic marine sediments: Evidence for a methanogen-sulfate reducer consortium, *Global Biogeochem. Cycles*, *8/4*, 451–463.
Hustoft, S., S. Bünz, J. Mienert, and S. Chand (2009), Gas hydrate reservoir and active methane venting province in sediments on 20 Ma young oceanic crust in the Fram Strait, offshore NW Svalbard, *Earth Planet. Sci. Lett.*, *284*, 12–24.
Ingólfsson, Ó., and J. Y. Landvik (2013), The Svalbard – Barents Sea ice-sheet – historical, current and future perspectives, *Quat. Sci. Rev.*, *64*, 33–60.
Jessen, S. P., T. L. Rasmussen, T. Nielsen, and A. Solheim (2010), A new Late Weichselian and Holocene marine chronology for the western Svalbard slope 30,000–0 cal years BP, *Quat. Sci. Rev.*, *29*, 1301–1312.
Kirschke, S., et al. (2013), Three decades of global methane sources and sinks, *Nat. Geosci.*, *6*, 813–823.
Kroopnick, P. (1985), The distribution of ^{13}C of ΣCO_2 in the world oceans, *Deep Sea Res., Part A*, *32*, 57–84.
Loeblich, A. R., Jr., and Tappan, H. (1953), Studies of arctic foraminifera, *Smithson Misc. Collect.*, *121*(7), 1–150.

Lucchi, R. G., et al. (2013), Postglacial sedimentary processes on the Storfjorden and Kveithola trough mouth fans: Significance of extreme glacimarine sedimentation, *Global Planet. Change*, *111*, 309–326.
Mangerud, J., and S. Gulliksen (1975), Apparent radiocarbon ages of recent marine shells from Norway, Spitsbergen, and Arctic Canada, *Quat. Res.*, *5*, 263–273.
Mangerud, J., T. Dokken, D. Hebbeln, B. Heggen, O. Ingolfsson, Y. J. Landvik, V. Mejdahl, J. I. Svendsen, and T. O. Vorren (1998), Fluctuations of the Svalbard-Barents Sea ice sheet during the last 150,000 years, *Quat. Sci. Rev.*, *17*, 11–42.
Mangerud, J., S. Bondevik, S. Gulliksen, A. Karin Hufthammer, and T. Høisæter (2006), Marine ^{14}C reservoir ages for 19th century whales and molluscs from the North Atlantic, *Quat. Sci. Rev.*, *25*, 3228–3245.
Marín-Moreno, H., T. A. Minshull, G. K. Westbrook, and B. Sinha (2015), Estimates of future warming-induced methane emissions from hydrate offshore west Svalbard for a range of climate models, *Geochem. Geophys. Geosyst.*, *16*, 1307–1323, doi:10.1002/2015GC005737.
Martin, R. A., E. A. Nesbitt, and K. A. Campbell (2010), The effects of anaerobic methane oxidation on benthic foraminiferal assemblages and stable isotopes on the Hikurangi Margin of eastern New Zealand, *Mar. Geol.*, *272*, 270–284.
Mattingsdal, R., J. Knies, K. Andreassen, K. Fabian, K. Husum, K. Grøsfjeld, and S. De Schepper (2014), A new 6 Myr stratigraphic framework for the Atlantic-Arctic Gateway, *Quat. Sci. Rev.*, *92*, 170–178.
Millo, C., M. Sarnthein, H. Erlenkeuser, and T. Frederichs (2005a), Methane-driven late Pleistocene δ^{13}C minima and overflow reversals in the southwestern Greenland Sea, *Geology*, *33*, 873–876.
Millo, C., M. Sarnthein, H. Erlenkeuser, P. M. Grootes, and N. Andersen (2005b), Methane-induced early diagenesis of foraminiferal tests in the southwestern Greenland Sea, *Mar. Micropaleontol.*, *58*, 1–12.
Müller, J., and R. Stein (2014), High-resolution record of late glacial and deglacial sea ice changes in Fram Strait corroborates ice-ocean interactions during abrupt climate shifts, *Earth Planet. Sci. Lett.*, *403*, 446–455.
Neretin, L., M. Böttcher, B. B. Jørgensen, I. I. Volkov, H. Lüschen, and K. Hilgenfeldt (2004), Pyritization processes and greigite formation in the advancing sulfidization front in the Upper Pleistocene sediments of the Black Sea, *Geochim. Cosmochim. Acta*, *68*, 2081–2093.
Nisbet, E. G., and J. Chappellaz (2009), Shifting gear, quickly, *Science*, *324*, 477–478.
Panieri, G. (2006), Foraminiferal response to an active methane seep environment: A case study from the Adriatic Sea, *Mar. Micropaleontol.*, *61*(1–3), 116–130.
Panieri, G., A. Camerlenghi, I. Cacho, C. S. Cervera, M. Canals, S. Lafuerza, and G. Herrera (2012), Tracing seafloor methane emissions with benthic foraminifera: Results from the Ana submarine landslide (Eivissa Channel, Western Mediterranean Sea), *Mar. Geol.*, *291–294*, 97–112.
Panieri, G., R. H. James, A. Camerlenghi, G. K. Westbrook, C. Consolaro, I. Cacho, V. Cesari, and C. Sanchez Cervera (2014), Record of methane emissions from the West Svalbard continental margin during the last 23,500 years revealed by δ^{13}C of benthic foraminifera, *Global Planet. Change*, *122*, 151–160.
Parmentier, F.-J. W., and T. R. Christensen (2013), Arctic: Speed of methane release, *Nature*, *500*, 529–529.
Pena, L. D., E. Calvo, I. Cacho, S. Eggins, and C. Pelejero (2005), Identification and removal of Mn-Mg-rich contaminant phases on foraminiferal tests: Implications for Mg/Ca past temperature reconstructions, *Geochem. Geophys. Geosyst.*, *6*, Q09P02, doi:10.1029/2005GC000930.
Piñero, E., M. Marquardt, C. Hensen, M. Haeckel, and K. Wallmann (2013), Estimation of the global inventory of methane hydrates in marine sediments using transfer functions, *Biogeosciences*, *10*, 959–975.
Plaza-Faverola, A., S. Bünz, J. E. Johnson, S. Chand, J. Knies, J. Mienert, and P. Franek (2015), Role of tectonic stress in seepage evolution along the gas hydrate-charged Vestnesa Ridge, Fram Strait, *Geophys. Res. Lett.*, *42*, 733–742, doi:10.1002/2014GL062474.
Rajan, A., J. Mienert, and S. Bünz (2012), Acoustic evidence for a gas migration and release system in Arctic glaciated continental margins offshore NW-Svalbard, *Mar. Pet. Geol.*, *32*, 36–49.
Rasmussen, S. O., et al. (2006), A new Greenland ice core chronology for the last glacial termination, *J. Geophys. Res.*, *111*, D06102, doi:10.1029/2005JD006079.
Rathburn, A. E., M. E. Pérez, J. B. Martin, S. A. Day, C. Mahn, J. Gieskes, W. Ziebis, D. Williams, and A. Bahls (2003), Relationships between the distribution and stable isotopic composition of living benthic foraminifera and coldmethane seep biogeochemistry in Monterey Bay, California, *Geochem. Geophys. Geosyst.*, *4*(12), 1106, doi10.1029/2003GC000595.
Ravelo, A. C., and C. Hillaire-Marcel (2007), The use of oxygen and carbon isotopes of foraminifera in paleoceanography, in *Proxies in Late Cenozoic Paleoceanography*, pp. 735–760, edited by C. Hillaire-Marcel and A. de Vernal, Elsevier, Amsterdam.
Reagan, M. T., and G. J. Moridis (2007), Oceanic gas hydrate instability and dissociation under climate change scenarios, *Geophys. Res. Lett.*, *34*, L22709, doi:10.1029/2007GL031671.
Reagan, M. T., and G. J. Moridis (2009), Large-scale simulation of methane hydrate dissociation along the West Spitsbergen Margin, *Geophys. Res. Lett.*, *36*, L23612, doi:10.1029/2009GL041332.
Rebesco, M., A. Wåhlin, J. S. Laberg, U. Schauerd, A. Beszczynska-Möllere, R. G. Lucchi, R. Noormets, D. Accettella, Y. Zarayskaya, and P. Diviacco (2013), Quaternary contourite drifts of the Western Spitsbergen margin, *Deep Sea Res., Part I*, *79*, 156–168.
Reimer, P. J., et al. (2013), INTCAL13 and MARINE13 radiocarbon age calibration curves 0–50,000 year Cal BP, *Radiocarbon*, *55*, 1869–1887.
Riedinger, N., K. Pfeifer, S. Kasten, J. F. L. Garming, C. Vogt, and C. Hensen (2005), Diagenetic alteration of magnetic signals by anaerobic oxidation of methane related to a change in sedimentation rate, *Geochim. Cosmochim. Acta*, *69*, 4117–4126.
Riedinger, N., S. Kasten, J. Gröger, C. Franke, and K. Pfeifer (2006), Active and buried authigenic barite fronts in sediments from the Eastern Cape Basin, *Earth Planet. Sci. Lett.*, *241*, 876–887.
Ritger, S., B. Carson, and E. Suess (1987), Methane-derived authigenic carbonates formed by subduction-induced pore-water expulsion along the Oregon/Washington margin, *Geol. Soc. Am. Bull.*, *98*, 147–156.
Rohling, E. J., and S. Cooke (2002), Stable oxygen and carbon isotopes in foraminiferal carbonate shells, in *Modern Foraminifera*, edited by B. K. Sen Gupta, pp. 239–258, Kluwer, Dordrecht, Netherlands.
Sahling, H., et al. (2014), Gas emissions at the continental margin west of Svalbard: Mapping, sampling, and quantification, *Biogeosciences*, *11*, 6029–6046.
Saloranta, T. M., and H. Svendsen (2001), Across the Arctic front west of Spitsbergen: High-resolution CTD sections from 1998–2000, *Polar Res.*, *20*, 177–184.
Sarkar, S., C. Berndt, T. A. Minshull, G. K. Westbrook, D. Klaeschen, D. G. Masson, A. Chabert, and K. E. Thatcher (2012), Seismic evidence for shallow gas-escape features associated with a retreating gas hydrate zone offshore west Svalbard, *J. Geophys. Res.*, *117*, B09102, doi:10.1029/2011JB009126.
Shakhova, N., et al. (2014), Ebullition and storm-induced methane release from the East Siberian Arctic Shelf, *Nat. Geosci.*, *7*, 64–70.

Skarke, A., C. Ruppel, M. Kodis, D. Brothers, and E. Lobecker (2014), Widespread methane leakage from the sea floor on the northern US Atlantic margin, *Nat. Geosci.*, *7*, 657–661.

Smith, A. J., J. Mienert, S. Bunz, and J. Greinert (2014), Thermogenic methane injection via bubble transport into the upper Arctic Ocean from the hydrate-charged Vestnesa Ridge, Svalbard, *Geochem. Geophys. Geosyst.*, *15*, 1945–1959, doi:10.1002/2013GC005179.

Solheim, A., E. S. Andersen, A. Elverhøi, and A. Fiedler (1996), Late Cenozoic depositional history of the western Svalbard continental shelf, controlled by subsidence and climate, *Global Planet. Change*, *12*, 135–148.

Spielhagen, R. F., K. Werner, S. A. Sørensen, K. Zamelczyk, E. Kandiano, G. Budeus, K. Husum, T. M. Marchitto, and M. Hald (2011), Enhanced modern heat transfer to the Arctic by warm Atlantic Water, *Science*, *331*, 450–453.

Steinle, L., et al. (2015), Water column methanotrophy controlled by a rapid oceanographic switch, *Nat. Geosci.*, *8*, 378–382.

Stuiver, M., P. J. Reimer, and R. W. Reimer (2014), CALIB Radiocarbon Calibration, Execute Version 7.0. [Available at: http://calib.qub.ac.uk/calib/.]

Svendsen, J. I., V. I. Astakhov, D. Y. Bolshiyanov, I. Demidov, J. A. Dowdeswell, V. Gataullin, C. Hjort, H. W. Hubberten, E. Larsen, and J. Mangerud (1999), Maximum extent of the Eurasian ice sheets in the Barents and Kara Sea region during the Weichselian, *Boreas*, *28*, 234–242.

Thatcher, K. E., G. K. Westbrook, S. Sarkar, and T. A. Minshull (2013), Methane release from warming-induced hydrate dissociation in the West Svalbard continental margin: Timing, rates, and geological controls, *J. Geophys. Res. Solid Earth*, *118*, 22–38, doi:10.1029/2012JB009605.

Torres, M. E. (2003), Is methane venting at the seafloor recorded by δ^{13}C of benthic foraminifera shells?, *Paleoceanography*, *18*(3), 1062, doi:10.1029/2002PA000824.

Torres, M. E., R. A. Martin, G. P. Klinkhammer, and E. A. Nesbitt (2010), Post depositional alteration of foraminiferal shells in cold seep settings: New insights from flow-through time-resolved analyses of biogenic and inorganic seep carbonates, *Earth Planet. Sci. Lett.*, *299*, 10–22.

Urey, H. C., H. A. Lowenstam, S. Epstein, and C. R. McKinney (1951), Measurement of paleotemperatures and temperatures of the Upper Cretaceous of England, Denmark, and the southeastern United States, *Geol. Soc. Am. Bull.*, *62*, 399–416.

Werner, K., R. F. Spielhagen, D. Bauch, H. C. Hass, and E. Kandiano (2013), Atlantic Water advection versus sea-ice advances in the eastern Fram Strait during the last 9 ka: Multiproxy evidence for a two-phase Holocene, *Paleoceanography*, *28*, 283–295, doi:10.1002/palo.20028.

Westbrook, G. K., et al. (2009), Escape of methane gas from the seabed along the West Spitsbergen continental margin, *Geophys. Res. Lett.*, *36*, L15608, doi:10.1029/2009GL039191.

Whiticar, M. J. (1999), Carbon and hydrogen isotope systematics of bacterial formation and oxidation of methane, *Chem. Geol.*, *161*, 291–314.

Winkelmann, D., and J. Knies (2005), Recent distribution and accumulation of organic carbon on the continental margin west off Spitsbergen, *Geochem. Geophys. Geosyst.*, *6*, Q09012, doi:10.1029/2005GC000916.

Wollenburg, J. E., M. Raitzsch, and R. Tiedemann (2015), Novel high-pressure culture experiments on deep-sea benthic foraminifera - Evidence for methane seepage-related δ^{13}C of *Cibicides wuellerstorfi*, *Mar. Micropal.*, *117*, 47–64.

Zamelczyk, K., T. L. Rasmussen, K. Husum, F. Godtliebsen, and M. Hald (2014), Surface water conditions and calcium carbonate preservation in the Fram Strait during marine isotope stage 2, 28.8–15.4 kyr, *Paleoceanography*, *29*, 1–12, doi:10.1002/2012PA002448.